BACHELOR'S DEGREE THESIS

Degree in Mathematics

Title: Study of calcium sparks and calcium wave propagation in cardiac cells

Author: Ferran Pla Fernández

Advisor: Blas Echebarria Domínguez

Department: Física

Academic year: 2016

UNIVERSITAT POLITÈCNICA DE CATALUNYA
BARCELONATECH
Facultat de Matemàtiques i Estadística

Universitat Politècnica de Catalunya
Facultat de Matemàtiques i Estadística

Treball Fi de Grau

Study of calcium sparks and calcium wave propagation in cardiac cells

Ferran Pla Fernández

Advisor: Blas Echebarría Domínguez

Dpt. de Física, UPC

I would like to thank Blas Echebarria for showing me an interesting and new world for me, meshing mathematics and biology. Although I have only seen the surface of this relationship, it fascinates me.

Abstract

Contraction of cardiac cells is initiated by an increase in the level of intracellular calcium concentration. The calcium response is the combination of the local stochastic release of tens of thousands of release sites. The possible responses range from sparks (local release) to a global calcium increase, passing from calcium waves that propagate along the cell. In this project we model the intracellular calcium dynamics as a network of excitable elements that fire stochastically, and study the occurrence of calcium waves and spark nucleation. In an initial part, we model the sparks of a homogeneous distribution of calcium nodes. We study the wave propagation of this model depending on properties accounting for the state of the heart. We develop a simplified mean-field theory which will shed light on various aspects of the dynamics of the model. In a second part, we proceed to add clustering onto our model, and with it, we study its new wave propagation and the dynamics of the model.

Key words: Calcium sparks, Ryanodine Receptors, calcium wave propagation

Contents

1. Introduction

Calcium (Ca) holds an essential role in a broad number of subcellular signaling processes. Such as: muscle contraction(considered in this work), cell proliferation, or gene transcription. The dependence on calcium of the beating mechanism in the heart has been known for decades. It is well accepted that intracellular calcium release from the *sarcoplasmic reticulum (SR)* is vital for cardiac muscle contraction.

Each beat of the heart involves five major stages. The first two stages, often considered together as the "ventricular filling" stage, involve the movement of blood from the atria into the ventricles. The next three stages involve the movement of blood from the ventricles to the pulmonary artery (in the case of the right ventricle) and the aorta (in the case of the left ventricle).

The first stage, " diastole," is when the semilunar valves (the pulmonary valve and the aortic valve) close, the atrioventricular (AV) valves open, and the whole heart is relaxed.

The second stage, "atrial systole," is when the atrium contracts, and blood flows from atrium to the ventricle.

The third stage, "isovolumic contraction" is when the ventricles begin to contract, the AV and semilunar valves close, and there is no change in volume.

The fourth stage, "ventricular ejection," is when the ventricles are contracting and emptying, and the semilunar valves are open.

During the fifth stage, "isovolumic relaxation time", pressure decreases, no blood enters the ventricles, the ventricles stop contracting and begin to relax, and the semilunar valves close due to the pressure of blood in the aorta.

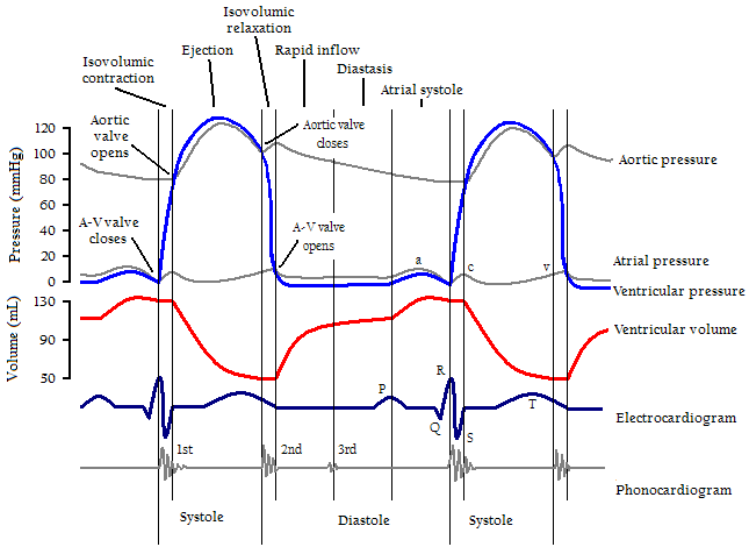

FIG. 1. Cardiac events occurring in the cardiac cycle. Two complete cycles are illustrated [**1**].

As shown in Fig 1, during the isovolumic contraction (third stage), there is a high increase in pressure, high volume and high electrical activity of the heart.

Calcium plays a particularly important role in the cardiac cell during the third stage as it mediates the coupling between membrane voltage and tissue contraction [**2**].

Presumably, a deficiency in signaling that prevents effective elevation of calcium would impair contractility as the contraction of heart muscle is directly determined by the level of calcium elevation during systole i.e. when the ventricles contract (see Fig. 2).

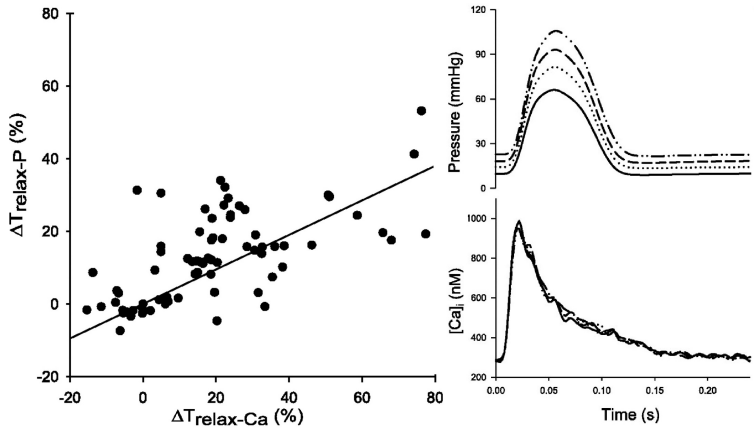

FIG. 2. The right picture shows the evolution of the calcium signals and pressure from the left ventricle during contraction. On the left, the paired values of pressure and Ca signals at a few points in time are illustrated [**3**].

Indeed, an appealing hypothesis for the mechanism underlying cardiac muscle dysfunction during heart failure, the leading cause of mortality in the developed world, is that impaired calcium release causes decreased muscle contraction (systolic dysfunction) and defective calcium removal hampers relaxation (diastolic dysfunction) [**4**]. Given that the measurement of cellular calcium is relatively straightforward, the obvious experiment required to address this important issue is to measure calcium in heart muscle cells from failing hearts. Such measurements have been done [**5**] and, though there is a fair amount of variability in the published reports, the data tend to support the concept of a decrease in SR calcium release and a defect in the termination of release. These results imply that there are presumably defects in SR calcium release.

A central role in Ca regulation is played by the *ryanodine receptor (RyR)* which controls the flow of Ca from intracellular Ca stores to the cell interior. An important feature of RyR channels is that they are highly sensitive to Ca and transition from a closed to open state in a Ca-dependent manner. This Ca sensitivity, is further amplified by the close arrangement of RyR channels into clusters of 10–100 RyR channels. This system ensures that small increases of local Ca concentration can trigger a wave of opening RyR channels, leading to a large local release of Ca.

In a cardiac cell there are several thousand of these clusters organized along equally spaced planes (Z planes) (see Fig 3), so that signaling is determined by the number and timing of these release events. Ca released at a given cluster can diffuse and activate its nearest neighbors. Thus, under certain conditions a fire-diffuse-fire wave can propagate in the cell. These Ca propagation events are referred to as *spontaneous Ca release (SCR)* since the release that occurs in this fashion is typically initiated by a random opening of a single or group of RyR clusters.

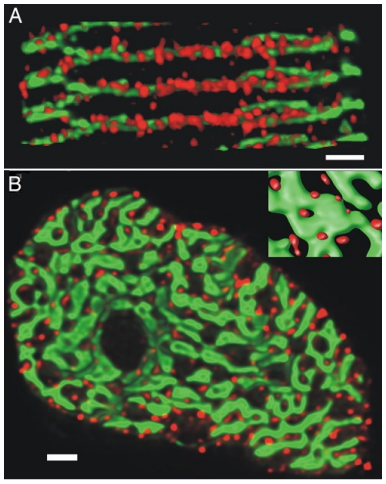

FIG. 3. RyR cluster distribution and relationship to z-plane structure. (A) Shown is the distribution of RyR clusters (red) and its relation to the location of z-disks (green) in a rat ventricular myocyte. Note how z-disks bifurcate and the RyR cluster distribution follows this architecture. (B) The transverse distribution of RyR clusters (red) in a rat myocyte in a complete z-disk around the myofibrils (green).

These spontaneous Ca waves play an important role in the genesis of cardiac arrhythmia since they can lead to membrane depolarization, which, if it occurs in a population of cells, can induce a focal excitation that propagates in heart tissue. These excitations are dangerous because their timing is random and they can therefore disrupt the regular beating of the heart and initiate cardiac arrhythmias. Despite a great deal of work the basic features of spontaneous Ca waves (SCR) are still not fully understood. While studies shed light on various aspects of sub-cellular Ca dynamics, several questions remain unanswered. For example, it is not known how the spatial distribution of calcium release units (CRUs) combines with fluctuations and excitability to determine the location of wave nucleation sites in the cell.

In this paper we explore a simplified theoretical model that can be used to understand essential features of Ca wave nucleation and propagation. We analyze in detail the role of the random arrangement of CRUs inside the cell, the strength of diffusive coupling, and the kinetics of spark activation and extinguishing. Our goal is to determine how these properties determine the location and timing of spontaneous Ca waves in cardiac cells. Using this approach, we show that the dynamics of SCR is crucially dependent on two important parameters. The first is the ratio of the length scale over which Ca diffuses from a Ca spark to the average distance between release sites in the cell, which gives a measure of the degree of coupling between CRUs in a cell. The second parameter is the amount of Ca released during a Ca spark, which determines the excitability of the system.

Part 1

Calcium release units (CRU) model

2. Introduction

In this section we will present a model used to study the relation between the arrangement of the calcium release units and the nucleation and propagation of Ca waves.

We aim to explore which parameters play a main role in the appearance of spontaneous calcium waves. According to many studies (see for instance [**7**]), there are a few parameters that have been established as having the biggest impact in these events:

- The spatial distribution of calcium release units: Modelling the interaction between adjacent CRUs is critically dependent on knowing the distance between one unit and its immediate neighbor.
- The excitability of the system: The amount of calcium released during a Ca spark regulates the propagating and nucleating of a wave.
- The ratio of the length scales: distances over which, Ca diffuses from a Ca spark to the average distance between release sites in the cell, which gives a measure of the degree of coupling between CRUs in a cell.

The first of these parameters was studied in [**7**]. In this project we plan to extend that work studying the effect of the other. To this end, we continue with the modelling of the system.

3. Model

First of all, our domain will consist of a 30 by 30 distribution of calcium release units, distributed homogeneously throughout $D = [0,1] \times [0,1]$. This is motivated by the cell physiology, where in a z-plane clusters of RyRs are distributed at an average distance of $0,5\mu m$ and the plane has approximate dimensions of $15\mu m \times 15\mu m$.

Since we are taking $[0,1]\times[0,1]$ all the length scales are rescaled. We are trying to emulate a distribution with no spatial irregularities. This way we will be able to observe the effect on the last two parameters (excitability and ratio of the length scales) clearly.

Given the complexity of the local RyR kinectics in a cluster, we will simplify the system by using a state variable η_i for each i^{th} CRU. This variable can be:

- $\eta_i = 0$, there is no spark in the i^{th} CRU.
- $\eta_i = 1$, there is spark in the i^{th} CRU.

To model the dynamics of Ca sparks we let the state variable follow a stochastic reaction scheme

$$\eta_i : 0 \underset{\beta_i}{\overset{\alpha_i}{\rightleftharpoons}} 1,$$

the process from no spark in the i^{th} cluster ($\eta_i = 0$), to a spark happening in the $CRU(\eta_i = 1)$, will happen at a certain rate that we define as α_i. This rate can depend on many properties of the cluster at every point in time, however, since RyR cluster openings are principally regulated by the local Ca concentration, we will take the forward rate to be:

$$\alpha_i = g_i c_i^2,$$

where c_i is the local calcium concentration and g_i is the excitability of the i^{th} CRU. We take a squared relationship with the Ca because is one of the simplest forms that actually approaches really accurately to the experimental data, recent experimental studies [**6**] reveal that the open probability of RyR channels is a highly nonlinear sigmoid function that we will use later on in this study.

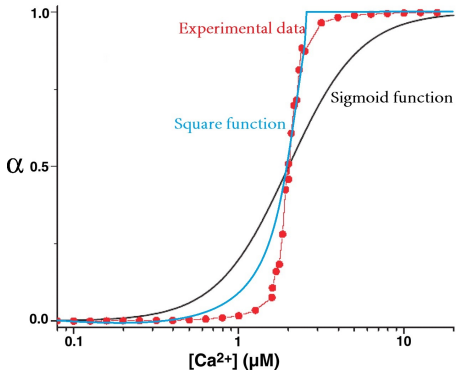

FIG. 4. Rate α in relation to the calcium concentration [**6**]. The red points are the actual found experimental points. We then illustrate a sigmoid function (black) and an artificial quadratic function (cian).

Besides, the CRU excitability is notably affected by the number of RyR in the cluster, in a latter chapter we will see how much.

The process of a spark closing in the i^{th} cluster ($0 \leftarrow 1$) will also happen at a certain rate, in this case we define it as β_i, which will be a fixed parameter, equal for every CRU.

In this model we are neglecting the slow recovery processes due to a previous excitation, so immediately after a CRU is closed, it can be reopened. The reason for such election is that we are just interested in the nucleation and propagation of Ca waves. As a result, having a rest constraint for every Calcium release unit will just add complexity to the system and will not give us any useful information.

The propagation of waves is caused by the following equation, expressing the local Ca concentration at a CRU [**7**]:

$$c_i(t) = c_0 + \sum_{j \neq i} h_{ij}(t)\eta_j(t), \tag{1}$$

where c_0 is the background Ca concentration, equal for every i^{th} CRU, h_{ij} is a kernel that accounts for the interaction between the local concentration at sites i and j. Having an opened CRU nearby influences positively on having a spark. This effect is proportional to the amount of Ca released at site j and inversely proportional to the distance between both units. The interaction is taken with a gaussian decay since we are considering diffusive coupling [**7**]:

$$h_{ij} = r_j e^{-\frac{(x_i - x_j)^2}{l^2}}, \tag{2}$$

where r_j represents the Ca released at the j^{th} CRU, x_i and x_j are the locations of both units and l is a diffusive length scale.

Summarizing, our model can be described with the following dynamic equations:

$$\begin{cases} \eta_i(t) : 0 \underset{\beta_i}{\overset{\alpha_i(t)}{\rightleftharpoons}} 1 \\ \alpha_i(t) = g_i c_i(t)^2 \\ c_i(t) = c_0 + \sum_{j \neq i} h_{ij} \eta_j(t) \\ h_{ij} = r_j e^{-\frac{(x_i - x_j)^2}{l^2}} \end{cases}$$

where:

$$\begin{cases} \alpha_i(t), \beta_i \in [0,1] \quad \forall i \\ c_0, l > 0 \\ r_i, g_i > 0 \quad \forall i \\ x_i \in [0,1] \quad \forall i \end{cases}$$

In the model there is a stochastic component that affects the whole system and as a result, the outcomes can vary from one simulation to another. We aim to study the expected behaviour of the nucleation and propagation of waves and want to extract as much of reliable information as possible. Therefore, this leads us to consider the time evolution of the probability of having an open CRU, i.e. the master equation.

4. Master equation

With understanding the basic features of the system as a target, we develop a simplified mean field theory which will clarify various aspects of the dynamics.

4.1. Master equation. First, we define the spark probability $P_i(t)$ to be the probability that the i^{th} CRU is active at time t, i.e., $\eta_i = 1$. The stochastic dynamics is then governed by:

The probability of the site being open at time t: $P_i(t)$ is the aggregate of:

- The probability of **opening** when it was **closed** at time $t - \tau$, which would be:

  $$[1 - P_i(t - \tau)](\alpha_i \tau),$$

  where $[1 - P_i(t - \tau)]$ is the probability of the site being closed at time $t - \tau$ and $(\alpha_i \tau)$ is the probability of the site i to transition from closed to open in time τ.
- The probability of **not closing** the site when it was **opened**:

  $$P_i(t - \tau)(1 - \beta_i \tau),$$

  where $P_i(t - \tau)$ is now the probability of the site being opened at time $t - \tau$ and $(1 - \beta_i \tau)$ is the probability of not closing the site i in time τ.

And so, we get to the known Master equation:

$$P_i(t + \tau) = [1 - P_i(t)](\alpha_i \tau) + P_i(t)(1 - \beta_i \tau) \tag{3}$$

4.2. Mean field approximation. To simplify the dynamics we make the approximation that the state variables can be replaced by their probabilities (averages) so that $\eta_i \approx P_j$, and the local calcium concentration can be approached by:

$$c_i \approx c_0 + \sum_{j \neq i} h_{ij} P_j(t).$$

Using that $\alpha_i = g_i c_i^2$ and replacing the last approximation in the equation we get:

$$P_i(t+\tau) = [1 - P_i(t)](g_i \left(c_0 + \sum_{j \neq i} h_{ij} P_j(t) \right)^2 \tau) + P_i(t)(1 - \beta_i \tau),$$

Developing this we get to:

$$P_i(t+\tau) - P_i(t) = \left([1 - P_i(t)](g_i \left(c_0 + \sum_{j \neq i} h_{ij} P_j(t) \right)^2) - P_i(t)\beta_i \right) \tau,$$

$$\frac{P_i(t+\tau) - P_i(t)}{\tau} = [1 - P_i(t)](g_i \left(c_0 + \sum_{j \neq i} h_{ij} P_j(t) \right)^2) - P_i(t)\beta_i,$$

And for a small enough τ, we conclude:

$$\frac{dP_i(t)}{d\tau} = [1 - P_i(t)][g_i \left(c_0 + \sum_{j \neq i} h_{ij} P_j(t) \right)^2] - P_i(t)\beta_i. \tag{4}$$

This last equation describes the time evolution of the spark probability $P_i(t)$. From here we can extract both the steady state points and their stability. Afterwards we can analyze the results which will help us understand the waves dynamics to a higher level.

Part 2

Homogeneous distribution of Calcium nodes

5. Wave nucleation and propagation

Initially, we will be simulating a basic nucleating and propagating of a wave in our domain.

5.1. System Parameters. We will take every unit property parameter equal for every CRU: $\alpha_i = \alpha$, $\beta_i = \beta$, $g_i = g$ and $r_i = r$ so that the heterogeneity in the system is passively originated by the stochastic processes for the Ca sparks.

To fix the system parameters, we rely on existing experimental results. For the excitability of a CRU we will fix the value at $g = 0.5ms^{-1}$ and the background calcium value at $c_0 = 0.01\mu M$. This will mean $\alpha \approx 0.001ms^{-1}$, which is approximately one spark every second. We will vary values for r and l, as a result we will be able to see the effect of both parameters on the nucleation and propagation of waves. The interaction of $CRUs$ will be given by the parameter r, and the diffusive length scale l. Finally, since a Ca spark typically lasts for a duration $20 - 50ms$ each, we will take $\beta = 0.05ms^{-1}$.

We will be processing all our models on the matlab platform, (the codes can be found in the last part of this study). We have many unknowns on our model that can fluctuate in a range of values, we will fix these parameters to be the mean of their fluctuations. This is the case of r and l. We fix these parameters to their average values:

$$r = 0.4, l = 3$$

Then, we will study wave propagation depending on the values of both of these parameters.

5.2. Simulation algorithm. The range of time will be of $1s$, which is expected to emerge one wave (for every ms we have the probability: $\alpha\Delta t = 0.001$, the chance of a wave not emerging is: $(1 - 0.001)^{1000} = 0.3676$ which means that approximately 2 out of 3 times, a wave will appear). What determines the time step is a range of values between which the rate $\alpha_i\Delta t$ does not surpass 1, small enough in order to have a high precision and big enough in favor of being a computationally feasible simulation. As a result, the time-step will be of $0.05ms$.

At every time-step we will:

- Update the Calcium at every Calcium Release Unit. At every time-step, we will use the local calcium effect equation:
$$c_i(t) = c_0 + \sum_{j \neq i} h_{ij}(t)\eta_j(t),$$
If a nearby site is open, it will have an increasing effect on the calcium.
- If $\eta_i = 0$ i.e, the site is closed, we will simulate a stochastic procedure of nucleating of wave: generate a random number $rand_i \in [0, 1]$ for every closed unit and nucleating a wave if this number is smaller than $rand_i < \alpha$. This will nucleate a wave at a site with probability α.
- If $\eta_i = 1$ i.e, the site is opened, we will simulate a stochastic procedure analogous to the previous one, but using β instead of α. This will close a site with probability β.
- Update the probability α. The amount of calcium at a site has a positive effect on the probability of nucleating a wave:
$$\alpha_i = g_i c_i^2$$

We then plot both the calcium and the η function at every step to follow the evolution of the waves.

5.3. Model results. This model in particular has some stochastic parameters and so, the results are less predictable than others: The wave can be nucleated at any point in our surface, the time at which wave is originated is also unpredictable and the way it dissipates can change at every iteration.

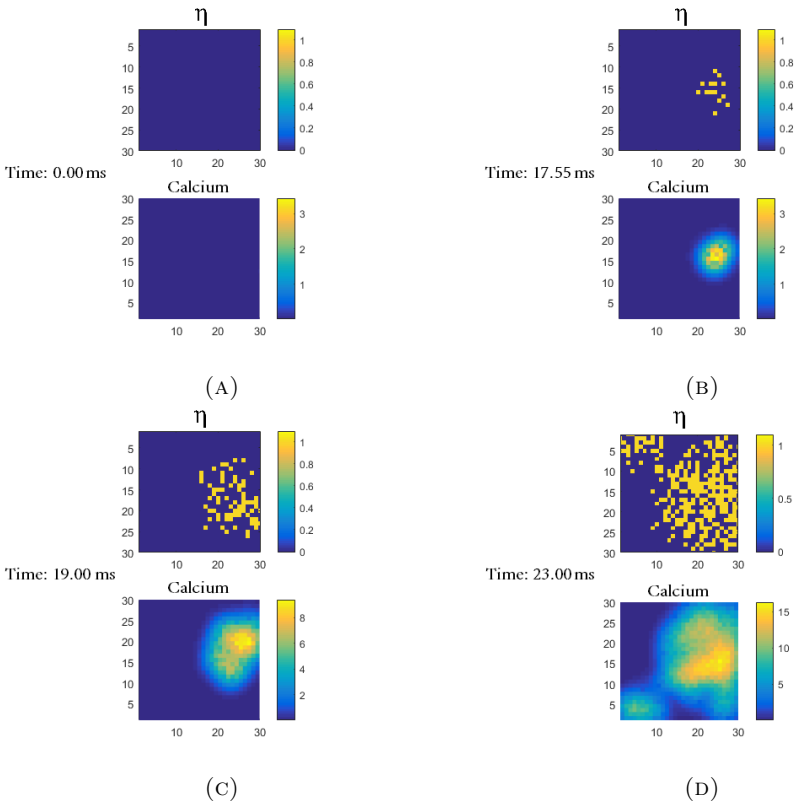

FIG. 5. (A): At the initial point in time, $\eta_i = 0$ for every calcium release unit, the system is at a rest steady state. The calcium for every i^{th} cluster is the background value, in this case is $c_0 = 0.01$. (B): At time $t = 17.05ms$, the first spark appears. Instants later, as we can see in the figure, the nearby $CRUs$ react to this nucleation and start sparking themselves. As the Calcium rises in a released unit, is diffused along the closer clusters. (C): At $t = 19.00ms$, the wave has propagated to one third of the whole surface, it has only been 1.95ms since the first spark appeared. We can see how the mirrored Calcium propagation agrees with the η nucleation. (D): After less than 6.00ms, the wave has propagated through most of the surface. It doesn't take long for the wave to propagate completely.

However, it is important to us the way this wave is propagated through the domain to understand the dynamics of the waves. Therefore, we capture four important points in time of a wave propagation:

We can extract from this that the wave is propagated in a diffusive manner, it doesn't take more than 10ms for the wave to propagate completely and if we had a resting constraint so that every node would require of a certain time to reopen again, we could see how it doesn't take more than 20ms for the wave to disappear.

We are keen on studying how this wave propagates in different situations, and subsequently we set the domain and the parameters to accomplish these tasks.

6. Wave propagation shape

Heart failures are frequently caused by an unsynchronized contraction, which can be induced by a pathological wave propagation, similarly, in a river, swirls are likely to appear in highly irregular terrains, and as a result, such river will not flow properly. One example of this is ventricular fibrillation (VF), it is the most serious cardiac rhythm disturbance. The lower chambers quiver and the heart can't pump any blood, causing cardiac arrest.

Following the same concept, we aim to study wave propagation in extreme conditions.

An important feature of the spatiotemporal dynamics is the nucleation of propagating Ca waves. To analyze the dynamics of these waves we consider the evolution of a planar front that joins a region of opened $CRUs$ with an inactive region. Our intention is to determine the conditions for which the planar front propagates and advances through our system.

First of all, let us consider the evolution of the planar front of active nodes

6.1. System Parameters. We will work with our previously fixed parameters except for the initial conditions.The position of each node i is (x_i, y_i) where $(x_i, y_i) \in [0, 1] \times [0, 1]$. Initial conditions are chosen such that:

$$\begin{cases} \eta_i = 1 & x_i \leq 0.5 \\ \eta_i = 0 & otherwise. \end{cases}$$

6.2. Evolution algorithm. We will be using the exact same algorithm as the one explained before. In this case we will use 4 checkpoints to show the evolution of the wave over time, these checkpoints will be:

- The initial state, when 50% of the sites are opened.
- 65% of the domain is opened.
- 75% is filled.
- Only 15% is closed.

With these checkpoints we will be able to reveal properties of the wave evolution.

6.3. Results. As seen in Fig 6, the wave spreads both rapidly and consistently, in less than 10ms, the wave has spread itself through nearly the entire domain.

As stated before, our objective is to determine at which conditions this front propagates and we have settled that the interaction between $CRUs$ and the effect of their neighbourhood (r), and the diffusive length scale (distance) are critical values on wave propagation.

7. Propagation study

Following this last statement we carry out the subsequent test: We will now vary both r and l between $[0.1, 1]$ and $[1, 5]$, respectively; and for each r and l we analyze whether this wave has spread or not. It takes a little more than a week to process this test with a considerable precision. Operating one single propagation of 100ms with the right accuracy takes approximately 2300 seconds and bearing in

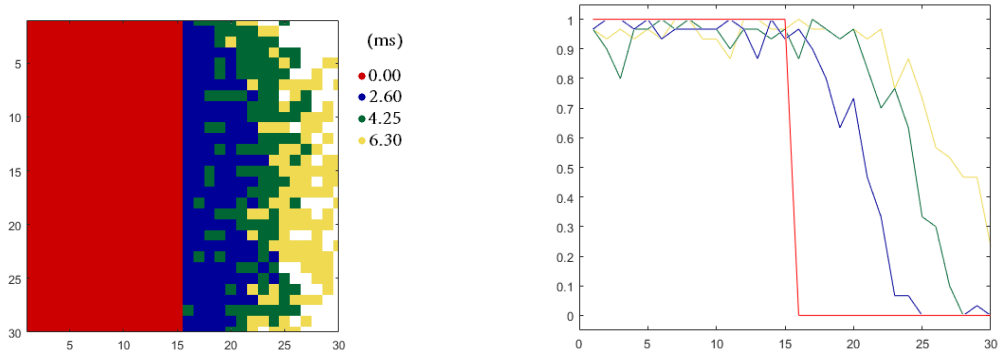

(A) (B)

FIG. 6. The evolution of a planar front of active sites. Four steps of the propagation are marked: The initial state(red), 65% of the domain is filled(blue), 75% is filled(green) and only 15% remaining (yellow). On the left(A), the painted area is where $\eta_i = 1$ in our domain. On the right(B), the amount of painted area(active sites) from (A), for each column of our domain, being 1 a completely opened column.

mind that to conclude the entire test, we need about 300 iterations, therefore, the process requires 200 hours of continuous processing, which is more than a week in a 8 Core 3.4 GHz processor.

Then we create the next function:

$$N'(r,l) = \sum_{i \in I} \eta_i$$

where I is the set of the array representing our domain. Utilizing this definition, we can obtain an indicator propagating function:

$$k(r,l) = \begin{cases} 1 & N'(r,l) \geq 3|I|/4 \\ 0 & otherwise. \end{cases} \tag{5}$$

Using this indicator, we build this last function:

$$f(r) = \sum_{l \in L} \frac{l \cdot (k(r,l) - (l - \Delta l) \cdot k(r, l - \Delta l))}{2} \tag{6}$$

where L is the set of l parameters that we are going to adopt. Therefore, $f(r) = l^*$ where l^* will be the median value l at which the wave will start spreading through more than three quarters of our domain.

7.1. System Parameters. The heterogeneity in the system will again be passively originated by the stochastic processes for the Ca sparks. All the parameters will be the same as in the previous planar front evolution (as it is what we keep studying). Except for three parameters:

- The interaction of $CRUs$ will vary the interval: $r \in [0.1, 1]$.
- The diffusive length scale will move between: $l \in [1, 5]$.
- We will not be looking at certain checkpoints, we will have a total time of $1s$.

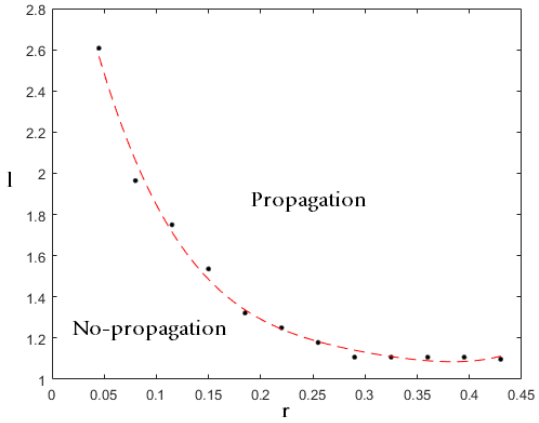

FIG. 7. We plot the function $f(r)$ and an exponential function approximation. This line separates the propagating and nonpropagating regions of phase space.

7.2. Propagation algorithm. We will be making an analogous propagation to the one in section 6.2.

- For every $r \in [0.1, 1]$ and $l \in [1, 5]$, we will process a simulation starting at the initial point and so, we will restart every parameter. At every iteration we:
  - Update the Calcium at every Calcium Release Unit. At every time-step, we will use the local calcium effect equation.
  - If $\eta_i = 0$ i.e, the site is closed, we will simulate a stochastic procedure of nucleating of wave with probability α.
  - If $\eta_i = 1$, we will simulate the closing of a wave with probability β.
  - Update the probability α. The amount of calcium at a site has a positive effect on the probability of nucleating a wave: $\alpha_i = g_i c_i^2$
- At the final point in time, we will be computing:

$$N'(r,l) = \sum_{i \in I} \eta_i$$

$$k(r,l) = \begin{cases} 1 & N'(r,l) \geq 3|I|/4 \\ 0 & otherwise. \end{cases}$$

- Finally, after having processed a simulation for every r and l, we are able to obtain:

$$f(r) = \sum_{l \in L} \frac{l \cdot (k(r,l) - (l - \Delta l) \cdot k(r, l - \Delta l))}{2} \quad \forall r \in [0.1, 1]$$

7.3. Study results. We obtain the results shown in Fig 7:

Our criterion for wave propagation is that more than 75% of the wave has successfully spread through the domain in less than 100ms. It is important to note that being the spreading process of less than 10ms, 100ms is more than enough to decide whether the wave has propagated or not.

In Fig 7 it is shown how highly dependant the wave propagation is on the system properties. If the neighbourhood interaction is too little, the wave will not propagate, as if the diffusive scale is small enough, it will not propagate either.

8. Steady state dynamics

To further characterize the dynamics we define the time dependant mean of active sites as:

$$\bar{N}(t) = \frac{\sum_{i=1}^{|I|} \eta_i}{|I|} \tag{7}$$

First of all, we will see how this equation evolves through time.

In order to accurately identify the keys of the system dynamics, we must take into account every important parameter.

One of these paramaters is that these dynamics depend crucially on initial conditions, particularly, the amount of active sites at the initial state. We will consider the dynamics for a broad range of initial conditions, from a completely absent state ($\bar{N}(0) = 0$), to a completely on state($\bar{N}(0) = 1$). The first of these conditions is far more reasonable and will be taken as the usual behaviour.

To begin with, we will take an experimental look at how the η function evolves through time depending on r (the interaction of CRUs). For low values of r we expect that $\bar{N}(t)$ (Eq. 7 denoting the number of open CRUs) will tend to 0, but as we increase r, $N(t)$ will start tending to 1.

8.1. System Parameters. As in the section 5.1, we will once again fix the diffusive scale at $l = 3$, naturally as it is the mean, from an experimental point of view. Besides r, all the other parameters will be the same as in previous simulations.

Secondly, the interaction of $CRUs$ will vary in the interval: $r \in [0.01, 1]$.

The evolution will be processed in a period of 200ms, which is enough time for the number of CRUs $\bar{N}(t)$ to stabilize.

Finally, we will take different initial conditions because we know that the initial state can have an important effect over the simulation. These initial states will be from an initial dark state: every site closed and as a result, $\bar{N}(0) = 0$; through various scaling steps of increasing the opened sites, which will be distributed randomly: $0 < \bar{N}(0) < 1$; to a full opened stated: $\bar{N}(0) = 1$.

8.2. Evolution algorithm. The process consists of two essential parts:

- The basic process of evolution and nucleation already done previously.
- The computation of $\bar{N}(t)$ at every time step (Eq. 7).

8.3. Study results. Plotting the evolution for various $r \in [0.01, 1]$ we end up discerning three different behaviours as shown in Fig 8.

- Consistently tending to a dark state (Fig 8a).
- Unstable and chaotic (Fig 8b).
- Consistently tending to an opened state (Fig 8c).

From this, we can extract that the steady dynamics will also have three different behaviours, and also, where will these behaviours occur.

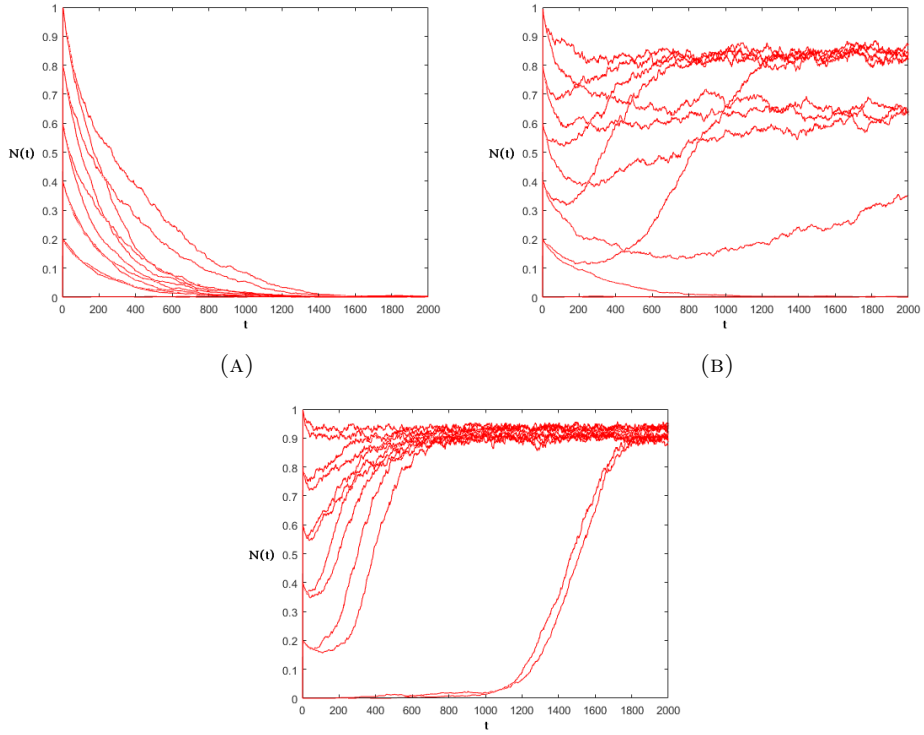

FIG. 8. Evolution over time of $\bar{N}(t)$ for different values of r. In (A) $r \in [0, 0.02]$, for (B) $r \in [0.03, 0.04]$ and in (C) $r \in [0.05, 1]$.

9. Master equation

Let us consider the spark probability $P_i(t)$. Using the model from section 4.2:

$$\frac{dP_i(t)}{d\tau} = [1 - P_i(t)][g_i\left(c_0 + \sum_{j \neq i} h_{ij} P_j(t)\right)^2] - P_i(t)\beta_i.$$

From here we aim to extract both the steady points and their stability.

In order to understand basic features of the system we develop a simplified mean field theory which will reveal various aspects of the dynamics. Then, we define the average spark probability:

$$\bar{P}(t) = \frac{1}{|I|} \sum_{i=1}^{|I|} P_i(t)$$

First of all, taking an experimental point of view, we compute the evolution of the ODE (Eq. 4) over time until it stabilizes. Consequently, we will get the strongest attracting points (if any) for which the probability stabilizes. We will compute an approximation of the fixed points as:

$$\bar{P}_\infty = \bar{P}(t \to \infty)$$

9.1. System Parameters. As in previous processes, we will be using most of the same parameters with a few variances, listed below.

As seen in the previous computation, the critical values for the interaction among sites will be between $r \in [0.01, 0.1]$. As a consequence, we will be computing $\bar{P}_\infty$ with $r \in [0, 0.5]$.

We will use various initial conditions in order to detect the different attracting points in the system. Particularly, we will be using 6 different initial points homogeneously distributed in $\bar{P}(0) \in [0, 1]$. Lastly, we will be processing the evolution of $\bar{P}$ up to 1000ms.

9.2. Mean field evolution algorithm. In favor of having a high precision in computing the evolution of this ODE, we decided to use a third order explicit Runge-Kutta method, defined by:

$$\begin{cases} y_{n+1} - y_n = \frac{h}{4}(k_1 + 3k_3) \\ k_1 = f(x_n, y_n) \\ k_2 = f(x_n + \frac{1}{3}h, y_n + \frac{1}{3}hk_1) \\ k_3 = f(x_n + \frac{2}{3}h, y_n + \frac{2}{3}hk_2) \end{cases} \tag{8}$$

Or defined by its *Butcher tableau*:

0	0		
1/3	1/3		
2/3	0	2/3	
	1/4	0	3/4

which is a third order method, and so, its error is $O(h^3)$. More precisely, in our experiments, $error \approx 0.1353h^3$. As a consequence, as we are using a step-size of 0.1, our error E, will be $|E| < 0.001$. We consider this as a good enough approximation.

In our case, we will be computing the evolution of every probability per site. In the master equation there is no explicit term for t, consequently, our method will change to:

$$\begin{cases} P_{i,n+1} - P_{i,n} = \frac{h}{4}(k_1 + 3k_3) \\ k_1 = f(P_{i,n}) \\ k_2 = f(P_{i,n} + \frac{1}{3}hk_1) \\ k_3 = f(P_{i,n} + \frac{2}{3}hk_2) \end{cases} \tag{9}$$

where $f(P_{i,n}) = \frac{dP_i(nh)}{d\tau}$. For every step we compute $\bar{P}(t)$ and we either stop at 10000 steps (1000ms) or when the mean $\bar{P}(t)$ stabilizes, i.e. it reaches an attracting point.

9.3. Results. As shown in Fig 9, we can observe part of a pitchfork bifurcation. There are three different behaviours (also expected from previous results):

- At very small values of $r \approx 0.02$, the interaction between sites is so limited that it barely has any effect, which makes the opening of a site implausible.
- At values between $r \in [0.05, 0.1]$ the probability becomes highly unstable and there are attracting points both at $\bar{P}_\infty = 0$ and at $\bar{P}_\infty = 1$.
- Finally, when r surpasses the 0.1 threshold, the interaction between sites is so powerful that it makes the probability of a site being open almost certainly 1.

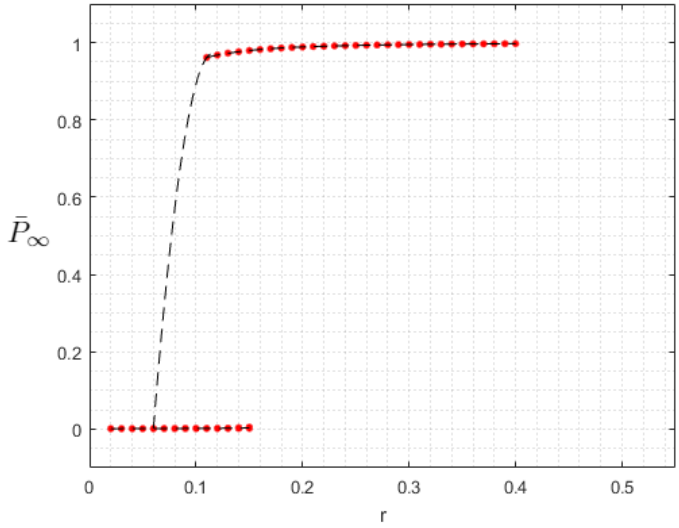

FIG. 9. Steady state values as a function of parameter r. Every point shown in red is where the mean of the probabilities per site stabilizes. Shown in a discontinuous line is an approximation of the expected analytical behaviour.

Our numerical analysis of the deterministic mean field equations reveals a complex behaviour. To analyze the transition from the stable solution $\bar{P}_\infty \approx 0$ to the unstable state, and then from the unstable state to the fully active state with $\bar{P}_\infty \approx 1$, we consider a linear stability analysis on the steady state points.

First, in response to our numerical solution not being the most precise, we initiate the linear stability study by getting a wider and higher precision set of steady state points.

10. Steady state points

The steady state points satisfy the following equations:

$$0 = f(P_i) = [1 - P_i][g_i\left(c_0 + \sum_{j \neq i} h_{ij} P_j\right)^2] - P_i\beta_i \quad \forall i \in I \tag{10}$$

Which is a system of 900 nonlinear equations. We aim to solve this system and later on, study the stability of its solutions.

10.1. System Parameters. We will have the same exact parameters used in the previous section. For us, $g_i = g, \beta_i = \beta, \forall i$. We will use the same structure for l and the initial conditions. In this case, r values will be focused between the transitions shown previously.

10.2. Algorithm. To solve this system we considered the Newton's Method. However, the computation cost of the jacobian matrix is rather high. As a result, we opted to use the Broyden's Method which is a quasi-Newton method, where instead of computing the jacobian matrix at every iteration,

we calculate this matrix at the first iteration and then use an estimate of the matrix by updating the one from the last iteration.

It is called a quasi-Newton method because it follows the secant matrix condition:

$$S_k \Delta x_k = \Delta f_k \tag{11}$$

where $\Delta x_k = x_k - x_{k-1}$ and $\Delta f_k = f_k - f_{k-1}$ and S_k is our approximation to the jacobian matrix $J(x_k)$. What Broyden's method adds to this equation is another condition to minimize the degrees of freedom and so, to be able to compute the S matrix.

The updating of the matrix is:

$$S_n = S_{n-1} + \frac{\Delta f_n - S_{n-1}\Delta x_n}{||\Delta x_n||^2}\Delta x_n \tag{12}$$

In our case, $x = P$ where $P = [P_0, P_1, ..., P_{900}]$, and our f is $f(P) = [f(P_0), f(P_1), ..., f(P_{900})]$, with f defined in Eq. 10.

In exchange of the far less expensive computation of the matrix, we loose both stability and convergence rate.

The Broyden method consists of:

(1) Stating an initial point P_0, computing its jacobian $J(P_0)$ and the error $E = ||f(P_0)||$.
(2) While the error is larger than the desired precision (in our case, we chose $E < 10^{-16}$), or we have surpassed the maximum of iterations (to avoid infinite loops, in our case maximum is 200), we:
   (a) Compute the following point:
   $$P_{k+1} = P_k - S_k^{-1} f(P_k)$$
   (b) Update the error:
   $$E = ||f(P_{k-1})||$$
   (c) Update the matrix S. In favor of simplicity, we can use point (a) and the equation (Eq. 12). Using $\Delta P_{k+1} = P_{k+1} - P_k$ and:
   $$S_k(P_{k+1} - P_k) = -f(P_k)$$
   into this equation:
   $$S_{k+1} = S_k + \frac{\Delta f(P_{k+1}) - S_k \Delta P_{k+1}}{||\Delta P_{k+1}||^2}\Delta P_{k+1}$$
   we get to:
   $$S_{k+1} = S_k + \frac{\Delta f(P_{k+1}) + f(P_k)}{||\Delta P_{k+1}||^2}\Delta P_{k+1}$$
   and finally, we update the matrix S using:
   $$S_{k+1} = S_k + \frac{f(P_{k+1})}{||\Delta P_{k+1}||^2}\Delta P_{k+1}$$
   (d) Update k: $k = k + 1$.

For every different r and initial condition P_0 we will process this algorithm and capture its resulting P^* when $k < 200$.

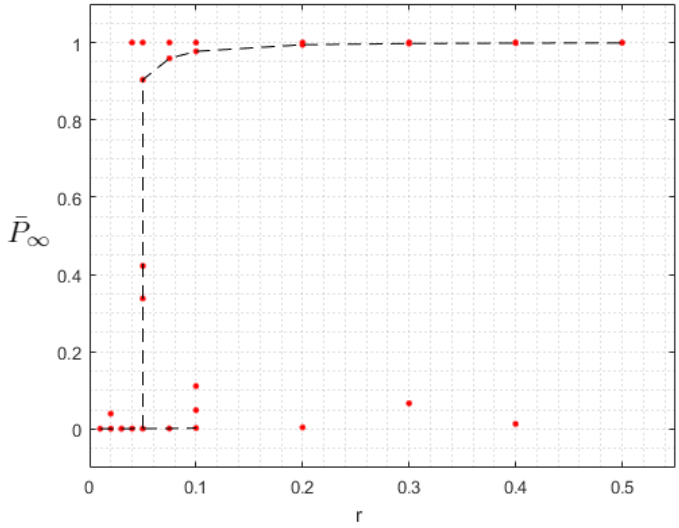

FIG. 10. Every point shown in red is where the mean of a steady point of the probabilities per site. Shown in a discontinuous line is where we see replicated the previous behaviour.

10.3. Results. As shown in Fig 10, there is a similar trend to the attracting points found in the previous computation (compare in Fig 9).

The points intersected by the discontinuous line are expected to be asymptotically stable. We will study their stability in order to identify whether they are stable, their convergence speed and direction.

11. Stability analysis

To analyze the transition that occurs between $r = [0.04, 0.07]$ we study the linear stability of the stable point $\bar{P}_\infty \approx 0$.

In this case, we expand Eq. 10 near the steady state solution: we define $P = P^* + e$ where P^* is the steady state solution and e is a small perturbation. For every $i \in I$, being p_i^* the i^{th} component of the steady state solution, we have $P_i = p_i^* + e_i$, where e_i is the small perturbation. Expanding to linear order in e_i:

$$\frac{dP_i}{dt} = \frac{dp_i^* + de_i}{dt} = [1 - p_i^* - e_i][g_i\left(c_0 + \sum_{j\neq i} h_{ij}(p_j^* + e_j)\right)^2] - (p_i^* + e_j)\beta_i.$$

Developing to linear order in e_i:

$$\frac{de_i}{dt} = -e_i[\beta_i + g_i\left(c_0 + \sum_{j\neq i} h_{ij}p_j^*\right)^2] + 2[1 - p_i^*][g_i\left(c_0 + \sum_{j\neq i} h_{ij}p_j^*\right)\sum_{j\neq i} h_{ij}e_j].$$

Thus, the stability of the low activity state is dictated by the system of equations $\frac{de_i}{dt} = \sum_j Q_{ij} e_j$ where

$$Q_{ij} = -[\beta_i + g_i\left(c_0 + \sum_{j\neq i} h_{ij} p_j^*\right)^2]\delta_{ij} + 2(1-p_i^*)[g_i\left(c_0 + \sum_{j\neq i} h_{ij} p_j^*\right)h_{ij}].$$

So we get to the following expression:

$$\frac{de}{dt} = Q \cdot e.$$

The time evolution of the system is then given by the linear combination

$$\vec{e}(t) = \sum_k a_k e^{\lambda_k t} \vec{\phi}_k$$

where λ_k and ϕ_k are respectively, the eigenvalues and the eigenvectors of the matrix Q. Through extracting both of these values we will be able to extract highly important information:

- Whether the quiescent state is asymptotically stable. Essentially, we will have to check whether the highest eigenvalue $\lambda' \geq \lambda_k, \forall k$ satisfies the condition $\lambda' \leq 0$
- Where is the nucleation of a wave the most probable to appear. In order to do so, we will check the distribution of weight in the eigenvector of the highest eigenvalue. As the highest eigenvalue is the least attracted to the inactive state, i.e. the most probable to nucleate a wave. Therefore, from the most probable to nucleate a wave we study the distribution in the eigenvectors, particularly, the highest eigenvector value will be the site with the highest chance to spark.

11.1. System parameters. It is important to note that the steady point that we will be studying is with $r = 0.05$ and its mean $\bar{P}_\infty = 0.0013$. Every other parameter is taken from previous methods.

11.2. System algorithm. First, we will simply determine the matrix Q by computing each of its components.

Secondly, we will substract both the eigenvectors and the eigenvalues of this matrix.

Finally, we will take the highest eigenvalue, check whether it is positive or not and afterwards we will check the distribution of its corresponding eigenvector. If it is positive, it will mean that the point is unstable, at least in a direction. If it is negative, this eigenvalue will be the slowest to converge in the paired eigenvector direction.

11.3. Results. The highest eigenvalue is $\lambda' = -0.0401$. Consequently, this point is asymptotically stable.

The eigenvector of this eigenvalue will be the slowest to converge, and as there is a chance for a wave to appear, this eigenvector will be the most probable to nucleate a wave. Studying the distribution of this eigenvector, we will be able to extract the specific areas from the domain where a wave is more likely to appear.

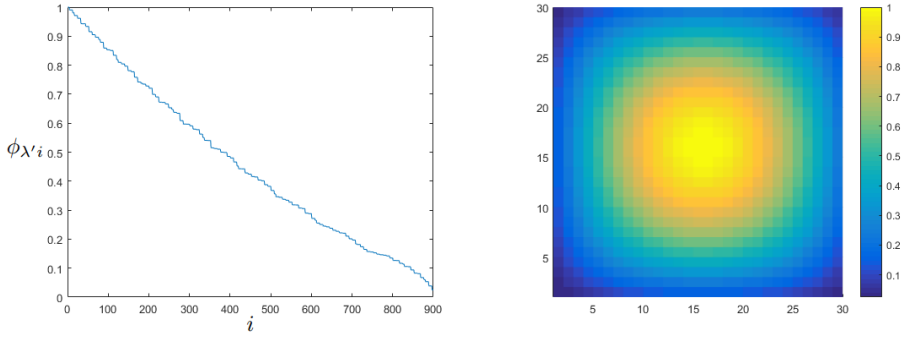

(A) (B)

FIG. 11. Distribution of the eigenvector from the highest eigenvalue. On the left (A), we show the relative values of the eigenvector, sorted from highest to lowest and normalized by the biggest value. On the right (B), we show the eigenvector value distribution over the domain (direction).

In Fig 11, we can see how the eigenvector of the highest eigenvalue has a heat-like distribution. In particular, the center of the domain has the highest probability to nucleate a wave and this probability diffuses homogeneously over the rest of the domain, reaching to the corners with the lowest probability.

Intuitively, the reason for this behaviour is that the site in the middle of the domain i^* is where the interaction between the rest of the sites is the highest because it has the minimum global distance between them. This makes h_{i^*j} of the site to be the biggest value of all h_{ij} and consequently, to have the highest α_{i^*} value.

11.4. Experimental nucleation. In order to verify our results, we have simulated 50000 wave nucleations. We have registered every site where the wave is nucleated.

In Fig 12 we can see how there is, although minimal, an increase of nucleations towards the middle of the domain.

In conclusion, we found out that the interaction between sites (r), the diffusive length scale (l) and the domain distribution of these sites, are important factors that affect both the nucleation and propagation of calcium waves.

In order to study the effect on a more complex clustered distribution, we will set calcium release units to have different properties. The number of RyRs per cluster follows an approximately exponential distribution with a mean RyR number of $13,6$ [**9**]. In the previous model we made every cluster to the same number of RyRs.

With this modification, we will have heterogeneous calcium release units which will get closer to the reality.

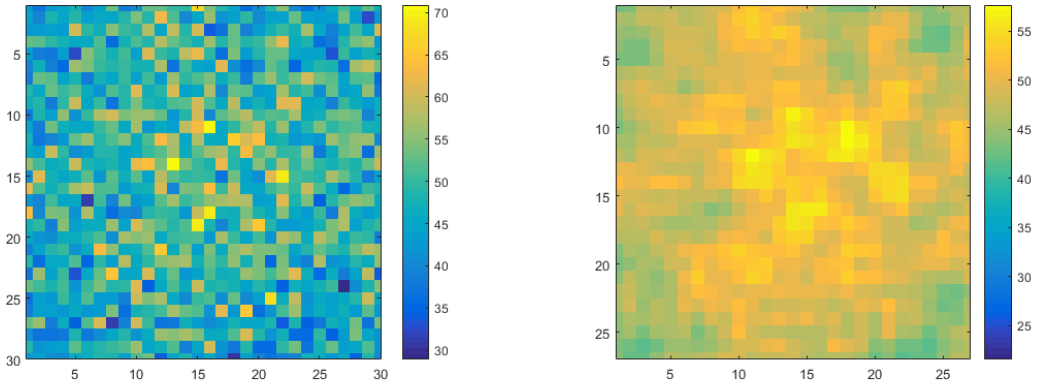

(A) (B)

FIG. 12. 50000 experimental nucleation of waves. On the left(A) we have the actual number of nucleations on every site. On the right(B), the accumulated number of nucleations over a 3 by 3 grid of sites.

Part 3

Heterogeneous distribution of Calcium nodes

12. Data generation

Initially, in order to simulate the RyR cluster distribution, we follow studies that have researched experimentally how the RyR clusters are distributed.

As shown in Fig 13 [**9**], the study carried out by the University of Pennsylvania Medical Center, reveals that the number of RyRs per cluster fits an exponential distribution.

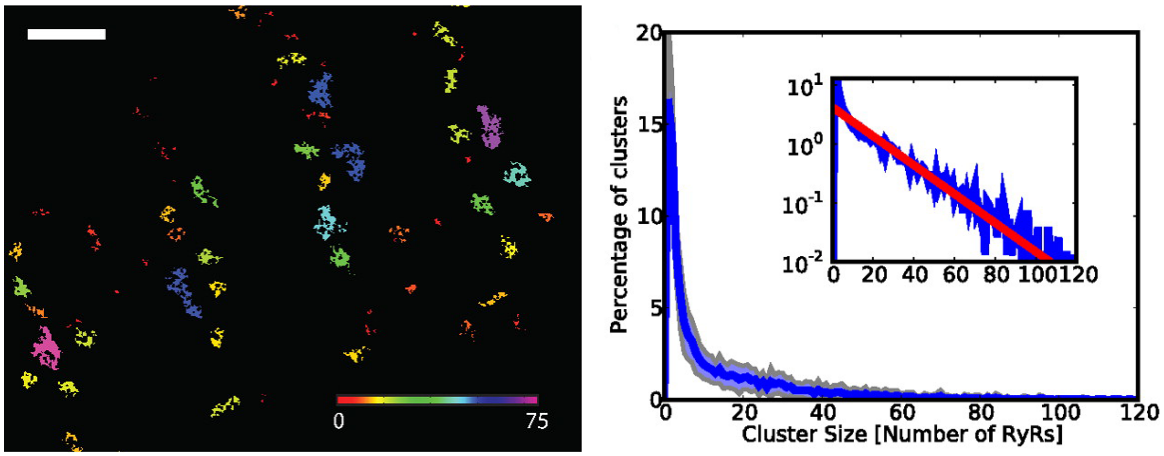

(A) (B)

FIG. 13. On the left, a region of the surface sarcolemma of a cardiac myocyte in which segmented RyR clusters are shown color-coded according to the number of RyRs they contain. Note the presence of many small clusters (red corresponds to number of RyR ≤ 7) (Scale bar, 1 μm.). On the right, the number of RyRs per cluster follows an approximately exponential distribution with a mean RyR number of 13.6. Shaded area represents the standard deviation. Inset: the same data on a log scale with a maximum-likelihood fit to an exponential distribution (red).

As a result, we have to generate 900 elements with an exponential distribution with mean $13,6$. As matlab does not have a free exponential distribution handling software, we will use the R platform to generate our data.

To transform this data into usable data for matlab, we will use both "Python" and internal matlab transformation functions to import data.

The number of RyRs in a cluster will affect directly to the excitability of that cluster, if there are more RyRs in a cluster, its excitability will increase. We will consider a linear relation between the number of RyRs in a cluster and its excitability, conserving its initial mean value: $\bar{g} = 0.5ms^{-1}$. For every CRU, we have:

$$g_i = \frac{0.5}{13.6} nc_i,$$

Where nc_i is the number of RyRs in the i^{th} CRU. With this, we compute g with the generated exponential distribution for the clusters.

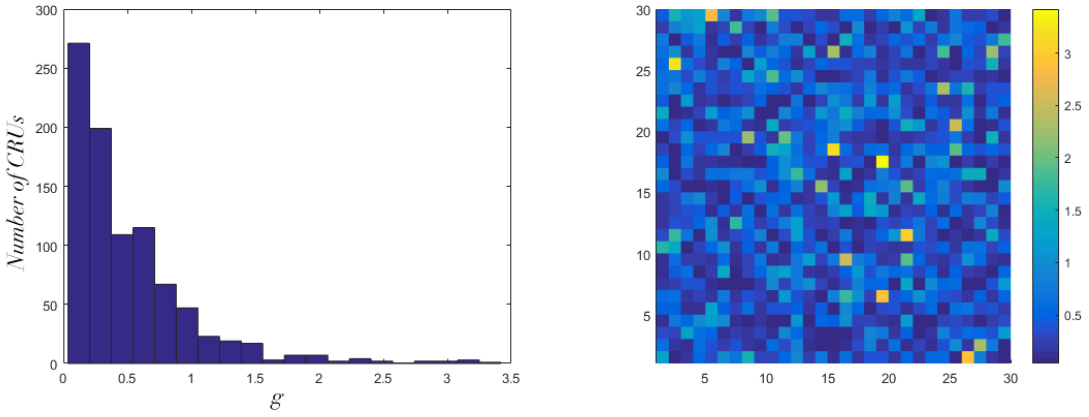

(A) (B)

FIG. 14. Excitability obtained from the exponential distribution generated for the clusters. On the left (A), we plot the histogram of its values with mean = 0.5. On the right (B), the distribution of g over the domain is shown.

In Fig 14 we show an example of a modified excitability with an exponentially distributed number of RyRs per cluster.

From this point onwards, we will be repeating the methods of study from the previous part with the aim of revealing the effect of the excitability variations among CRUs. We will only be updating the parts where the two models differ.

13. Wave nucleation and propagation simulation

13.1. System Parameters. In this instance, the heterogeneity of the system will be accentuated by the excitability as $g_i \neq g_j$ if $nc_i \neq nc_j$. Every other parameter will remain the same.

13.2. Simulation algorithm. There will be no modifications.

13.3. Model results. In Fig 15 we observe no clear differences between this model and the one we studied previously.

14. Wave propagation shape

14.1. System Parameters. We will work with our previously fixed parameters except for the initial conditions. For the initial conditions, we will repeat the process done in the same section from the previous part.

14.2. Planar front algorithm. Same as in section 6.2.

14.3. Results. As shown in Fig 16 and comparing it to Fig 6, there are no detectable differences between the two different models.

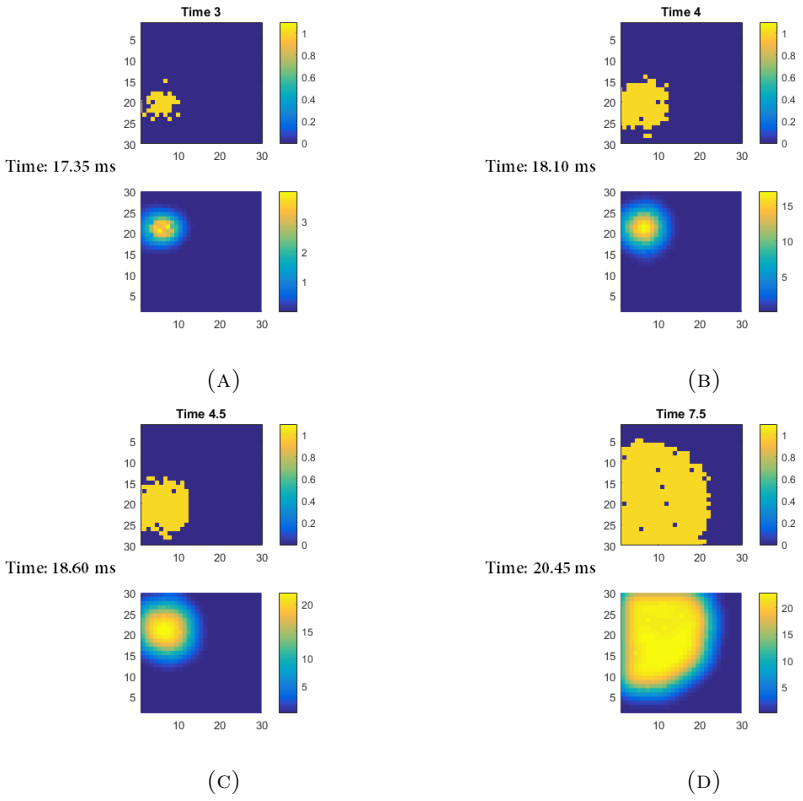

(A) (B) (C) (D)

FIG. 15. Four steps of the nucleation (A) and propagation of a wave (B), (C) and (D) with heterogeneous clusters.

15. Propagation study

15.1. System Parameters. As in section 7, we will be using the same parameters from the previous section 14.1 and will be changing:

- The interaction of $CRUs$ will vary in the interval: $r \in [0.1, 1]$.
- The diffusive length scale will move between: $l \in [1, 5]$.
- We will not be looking at certain checkpoints, we will consider a total time of $1s$.

15.2. Propagation algorithm. Cloned algorithm from the section 7.2.

15.3. Study results. Displayed in Fig 17 and comparing with Fig 7 we can see some minor changes, the propagation of the wave stabilizes faster, but overall, it stays the same.

16. Steady state dynamics

16.1. System Parameters. Apart from the different distribution for the excitability, all the parameters will be taken from section 8.1.

16.2. Experimental algorithm. Section 8.2.

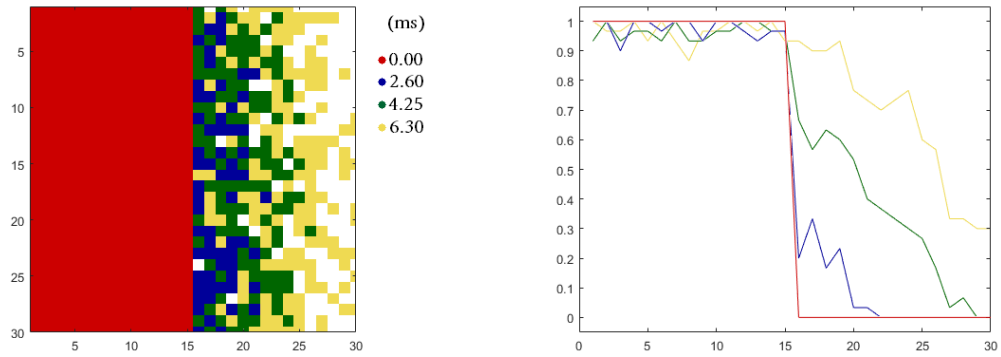

(A) (B)

FIG. 16. The evolution of a planar front of active sites. Four steps of the propagation are marked: The initial state(red), 65% of the domain is filled(blue), 75% is filled(green) and only 15% remaining (yellow). On the left(A), the painted area is where $\eta_i = 1$ in our domain. On the right(B), the amount of painted area(active sites) from (A), for each column of our domain.

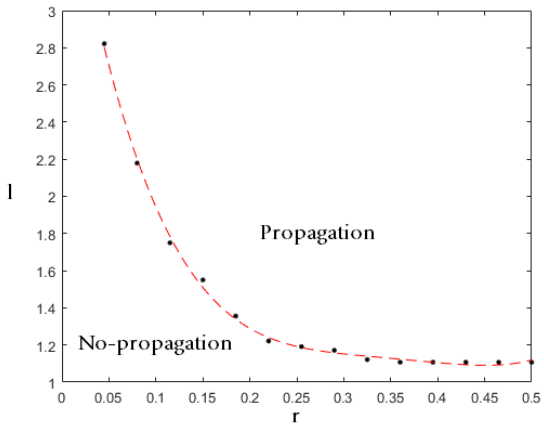

FIG. 17. Threshold over which the waves propagate over the domain, depending on r and l. Shown in black points are the actual experimental values from our simulations and shown in a discontinuous line is the expected border of the system.

16.3. Study results. As in the previous model, when plotting in Fig 18 the evolution for various $r \in [0.01, 1]$ we end up discerning three different behaviours:

- Consistently tending to a dark state, as seen in Fig 18a.
- Unstable and chaotic, as seen in Fig 18b.
- Consistently tending to an opened state, as seen in Fig 18c.

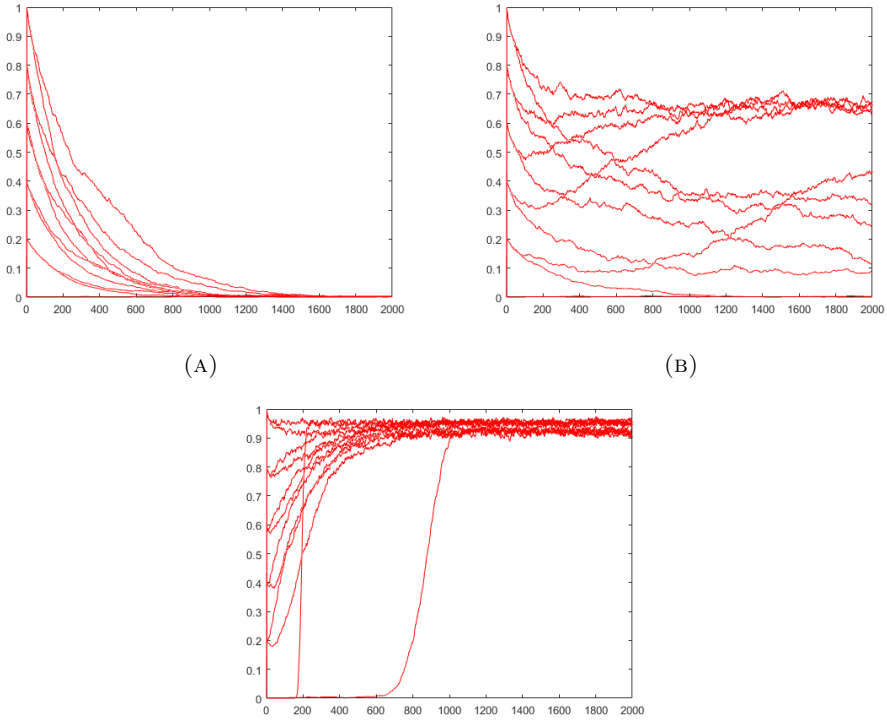

(A) (B)

(C)

FIG. 18. Evolution over time of N(t) for different values of r. In (A) $r \in [0, 0.02]$, for (B) $r \in [0.03, 0.04]$ and in (C) $r \in [0.05, 1]$.

17. Master equation

17.1. System Parameters. To fix the parameters we will repeat the process from section 9.1.

17.2. Mean field evolution algorithm. In favor of consistency and as it was successful in section 9.2, we will again use an explicit third order Runge-Kutta algorithm in order to follow the evolution of the probability.

17.3. Results. Shown in Fig 19, we can again observe part of a pitchfork bifurcation comparable to Fig 9. However, in this case, for $r > 0.3$ the fixed point becomes unstable and has problems converging.

18. Steady state points

18.1. System Parameters. We will have the same exact parameters used in section 17.1. Now, $g_i \neq g_j$ unlike before. However, $\beta_i = \beta, \forall i$. We will use the same structure for l and the initial conditions. In this case, the values of r will be chosen between the transitions shown previously.

18.2. Algorithm. In section 10.2, we used the Broyden's method. Although when replicating this algorithm for this model found the stable points, it had convergence problems in the unstable points

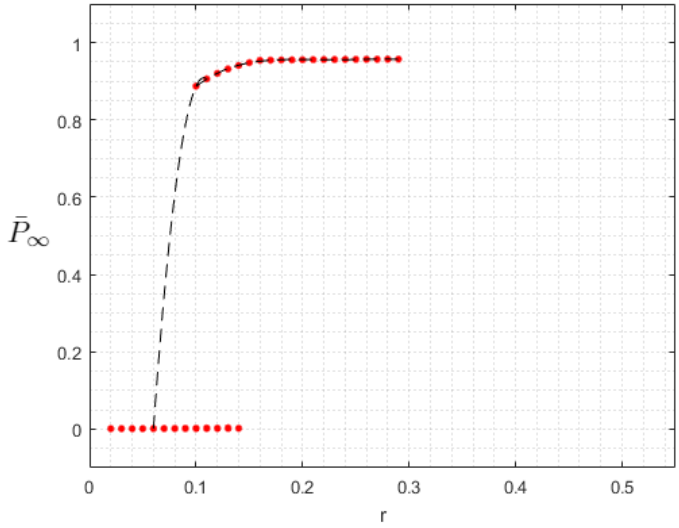

FIG. 19. Every point shown in red is where the mean of the probabilities per site stabilizes. Shown in a discontinuous line is an approximation of the expected analytical behaviour.

because the artificial Jacobian update was not as accurate as before. This inaccuracy was caused by the fact that from site to site the behaviour was immensely distant.

In order to get the unstable points, we used an artificial Bisection method:

(1) Developing a fine grid in the interval $P_\infty \in [0, 1]$
(2) Evaluating the function in these points:

$$f'(P_i) = [1 - P_i](g_i\left(c_0 + \sum_{j \neq i} h_{ij} P_j\right)^2) - P_i\beta_i \quad \forall i \in I$$

and keeping the points with sign changes between them.
(3) For each pair of points (P_0, P_1) where they have different signs:
   (a) Compute the following point:

$$P_3 = \frac{P_0 + P_1}{2}$$

   (b) If $f(P_3)$ is the desires steady point, STOP. Otherwise:

$$\begin{cases} P_0 = P_3 & P_0 P_3 > 0 \\ P_1 = P_3 & Otherwise. \end{cases}$$

   (c) Repeat from (a).

18.3. Results. As shown in Fig 20, there is a similar trend to the attracting points found in the previous computation, and comparable to Fig 10, it has the same behaviour. The unstable behaviour appears in a lower interaction for CRUs compared to the initial model.

We will study their stability in order to identify whether they are stable, their convergence speed and direction.

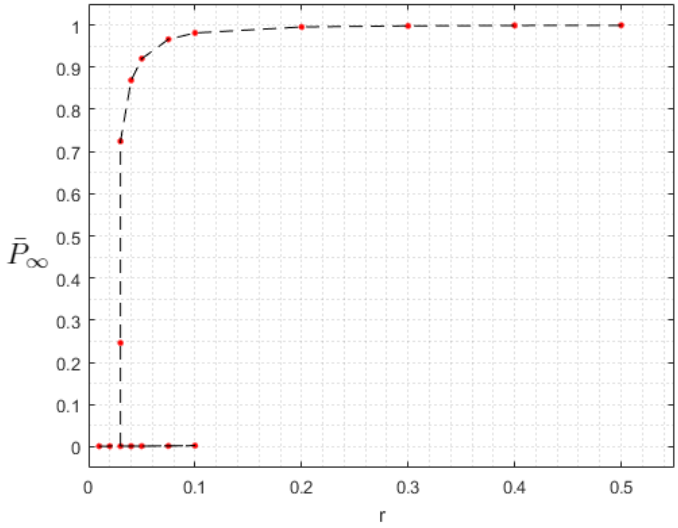

FIG. 20. Every point shown in red is where the mean of a steady point of the probabilities per site. Shown in a discontinuous line is where we see replicated the previous behaviour.

19. Stability analysis

To analyze the transition that occurs between $r = [0.03, 0.05]$ we study the linear stability of the fixed point $\bar{P}_\infty \approx 0$.

19.1. System parameters. It is important to note that we will be studying two fixed points:

- $r = 0.01$ and its mean $\bar{P}_\infty = 0.00106$. Expected to be asymptotically stable.
- $r = 0.03$ and its mean $\bar{P}_\infty = 0.24597$. Expected to be unstable.

Every other parameter is taken from previous methods.

19.2. System algorithm. Taken from section 11.2.

19.3. Results. For the first point, the highest eigenvalue is $\lambda' = -0.0471$. Consequently, this point is asymptotically stable.

For the second point, the highest eigenvalue is $\lambda' = 0.0436$. Consequently, this point is not stable.

From Fig 21 and Fig 22 we can see a completely different behaviour than from the previous model.

First, the eigenvector is much more focalized in a few sites. Secondly, it is an asymmetrical distribution.

Both of these facts are caused by the addition of the proximity between sites (which is what exclusively affected the previous model) and the excitability in those sites. The probability of a site opening is multiplied by both of these factors which makes the differences wider, thus the focalized values. The location of the highest values is determined by the global distance between the sites and its excitability. We can identify how the variations in the distribution of the eigenvector values agrees

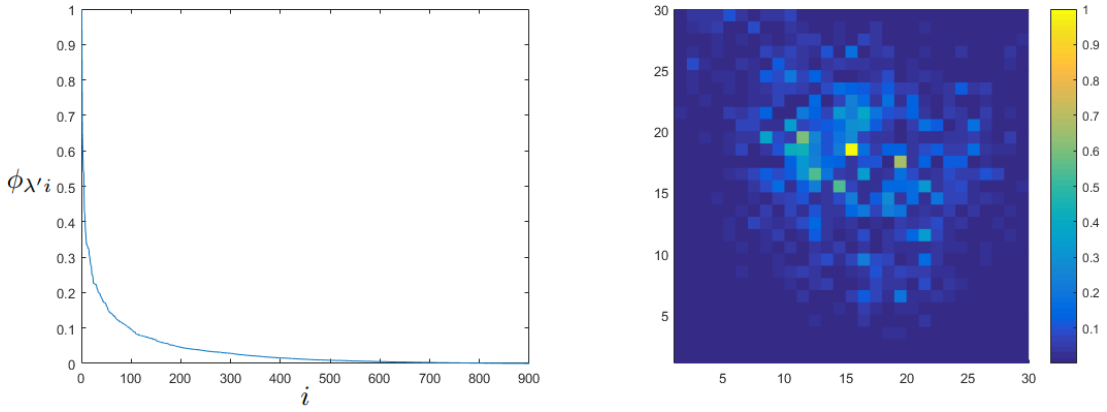

(A) (B)

FIG. 21. Distribution of the eigenvector from the highest eigenvalue for $r = 0.01$. On the left (A), we show the relative values of the eigenvector, sorted from highest to lowest and normalized by the biggest value. On the right (B), we show the eigenvector value distribution over the domain (direction).

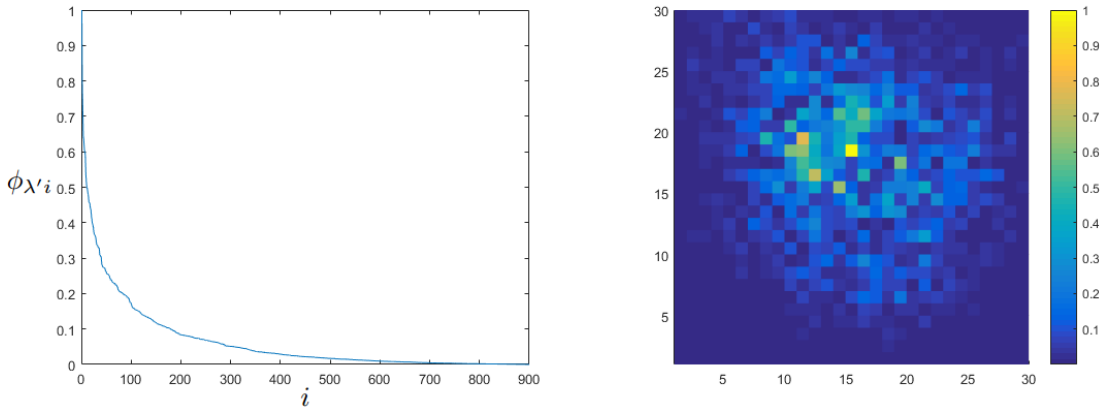

(A) (B)

FIG. 22. Distribution of the eigenvector from the highest eigenvalue. On the left (A), we show the relative values of the eigenvector, sorted from highest to lowest and normalized by the biggest value. On the right (B), we show the eigenvector value distribution over the domain (direction).

with the variations in the distribution of the generated excitability (g) comparing Figs 21 and 22 to Fig 14b.

19.4. Experimental nucleation. In order to verify our results, we will simulate 50000 wave nucleations. We will register every site where the wave is nucleated.

In Fig 23 we can see how there is, although minimal, an increase of nucleations towards the middle of the domain.

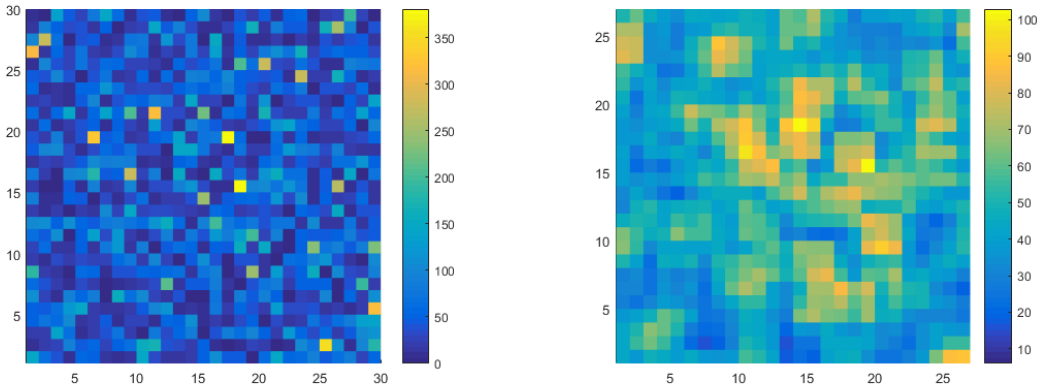

(A) (B)

FIG. 23. 50000 experimental nucleation of waves. On the left(A) we have the actual number of nucleations on every site. On the right(B), the accumulated number of nucleations over a 3 by 3 grid of sites.

Part 4

Conclusions

In this end-of-degree project, we have studied the process that involves the tissue contraction on the third stage of the cardiac cycle ("isovolumic contraction"). More precisely, we have taken into consideration the calcium signaling process, because the contraction of heart muscle (third stage) is directly determined by the level of calcium elevation during systole, i.e. when the ventricles contract.

A central role in calcium regulation is played by the ryanodine receptors, which control the flow of calcium from intracellular calcium stores, to the cell interior. In order to study calcium elevation process, we have recreated the mechanism produced in a z-plane (which is where thousand of RyRs are distributed in a cardiac cell).

In the first part of this project, we developed the model that we later used to simulate the process that involves the opening and closing of calcium release units (CRUs). In addition, we defined the master equation which in later stages, was studied to clarify various aspects of the dynamics.

Then, in the second part, we modeled a homogeneous distribution of CRUs in a z-plane, which shed light the properties that had a higher effect on an equally distributed domain. Notably, the neighbourhood interaction and the diffusive scale as the essential properties.

In the last part, we introduced heterogeneity in the cluster distribution on the CRUs in the plane. Consequently, we revealed that the number of RyRs in a cluster is a fundamental property in the nucleation and distribution of calcium waves.

Finally, a complementary study would be an improved version of this model. For example, we could add heterogeneity in the spatial distribution. Furthermore, we could also add size to the ryanodine receptors.

Part 5

Appendix

20. Matlab codes

We will be adding the main algorithms used in this project, not adding miscellaneous code (for data management, graphic details,...) nor parameter values assignments.

20.1. Wave nucleation and propagation. Algorithm in section 5.2.

```
for t = 2:steps
    %Update the calcium
    for i = 1:n
        calcium(i,t) = calcium(i,1);
        for j= 1:n
            if i ~= j
                calcium(i,t) = calcium(i,t) + h(X(i,:),X(j,:))*eta(j);
            end
        end
    end
    %Stochastic process, generate two random vectors
    ralpha = rand(n,1);
    rbeta = rand(n,1);
    %Stochastic process, spark process
    for i = 1:n
        if eta(i) == 0
            if ralpha(i) < alpha(i)*dt
                eta(i) = 1;
            end
        else
           if rbeta(i) < beta(i)*dt %<1
                eta(i) = 0;
           end
        end
    end

    %Plot the calcium and eta for every CRU
    figure(1);
    subplot(2,1,1);
        imagesc(reshape(eta(:),30,30));
        view(2);
        shading flat;
        caxis([-.01 1.1]);
        colorbar;
        axis([1 30 1 30]);
        title(sprintf('Time %g',dt*(t)))
        pause(0.01)

    subplot(2,1,2);
        surf(reshape(calcium(:,t),30,30));
        view(2);
        shading flat;
        colorbar;
```

```
        axis([1 30 1 30]);
        title(sprintf('Calcium'))
        pause(0.01)

    %Update alpha
    alpha = g.*calcium(:,t).^2;
end
```

Where $calcium(i,t) = c_i(t)$, $X(i,:)$ is the point of the i^{th} CRU, $eta(i) = \eta_i$, $alpha(i) = \alpha_i$, $beta(i) = \beta_i$ and $dt = \Delta t$. We also have $h(x_i, x_j) = h_{ij}$ as the following auxiliar function:

```
function f = h(xi,xj)
    r = 0.4;
    l = 3;
    f = r*exp(-norm(xi-xj)^2/l^2);
end
```

20.2. Propagation study. Algorithm in section 7.2.

```
for rind = 1:it1
    for lind = 1:it2
        calcium = zeros(n,2);

        %Initial values
        r = rvec(rind);
        l = lvec(lind);
        calcium(:,1) = 0.01;
        g = 0.5*ones(n,1);
        alpha = g.*calcium(:,1).^2;
        nu = zeros(n,1);
        nu(1:n/2,1) = ones(n/2,1);
        beta = 0.05*ones(n,1); %1??
        t = 1;

        %Process
        for t = 2:Steps
            for i = 1:n
                calcium(i,2) = calcium(i,1);
                for j= 1:n
                    if i ~= j
                        calcium(i,2) = calcium(i,2) + h2(X(i,:),X(j,:),r,l)*nu(j);
                    end
                end
            end

            ralpha = rand(n,1);
            rbeta = rand(n,1);

            for i = 1:n
                if nu(i) == 0
                    if ralpha(i) < alpha(i)*dt %<1
```

```
                        nu(i) = 1;
                    end
                else
                    if rbeta(i) < beta(i)*dt %<1
                        nu(i) = 0;
                    end
                end
            end

            %Update alpha
            alpha = g.*calcium(:,2).^2;
        end

        %Shaping into matrix
        eta=reshape(nu,n1,n1);
        eta2=sum(eta(:,1:n1))/n1;

        %Checking if propagated
        if sum(eta2) >= 15
            A(rind,lind) = 1;
        end
    end
end
```

Where $rvec$ and $lvec$ are the values tested for the propagation, we end up with a matrix A, where $A(r,l) = 0$ if the matrix has not propagated and $A(r,l) = 1$ otherwise. We also have h_{ij} depending on r and l: $h2(x_i, x_j, r, l) = h_{ij}$.

```
function f = h2(xi,xj,r,l)
    f = r*exp(-norm(xi-xj)^2/l^2);
end
```

20.3. Steady state dynamics. Algorithm in section 8.2. For every value r and initial value P, we reproduce the previous method and compute $\bar{N}(t)$:

```
eta_mean(t,P) = sum(eta)/n;
```

20.4. Master equation. Runge-Kutta algorithm in section 9.2.

```
while t <= 1000 || (dif >= 1e-6 && t < pasos)
    t = t + 1;
    for i = 1:n
        k1 = f2(i,n,P(i, t-1),P(:,t-1),X,beta(i),r)';
        k2 = f2(i,n,P(i, t-1) + (dt/3)*k1,P(:,t-1),X,beta(i),r)';
        k3 = f2(i,n,P(i, t-1) + (2*dt/3)*k2,P(:,t-1),X,beta(i),r)';
        P(i,t) = P(i,t-1) + (dt/4)*(k1 + 3*k3);
    end
    P2 = mean(P(:,t));
    dif = abs(P1 - P2);
    P1 = P2;
end
```

Where $f2 = f$:

```
function f = f2(i,n,Pi,P,X,beta,r)
    k = 0.01;
    g = 0.5;
    for j = 1:n
        if j ~= i
            k = k + h2(X(i,:),X(j,:),r)*P(j);
        end
    end
    fun = g*(k^2)*(1 - Pi) - beta*Pi;
end
```

20.5. Steady state points. Broyden algorithm in section 10.2.

```
while error > 10^-16 && k < 200
   k = k +1;
   incP1 = S\(-f(P1,X,rs(j)));
   P2 = P1 + incP1;
   %Stability boundaries
   P2(P2>1) = 1;
   P2(P2<0) = 0;
   S = S + (f(P2,X,rs(j))*incP1')/norm(incP1)^2;
   r(k) = norm(f(P2,X,rs(j)));
   P1=P2;
   iter(k)=k;
   error = r(k);
end
```

Where $error = E$, S is the artificial jacobian matrix, $P2 = P_{k+1}$ $P1 = P_k$. We also define $incP1 = \Delta P_{k+1}$.

20.6. Stability analysis. Algorithm in section 11.2.

Computing matrix Q:

```
for i = 1:n
    for j = 1:n
        if i == j
            Q(i,j) = -(beta + g*(c0 + hvector(i,X,r)*P)^2) + 2*g*(1-P(i))*(c0 +
            hvector(i,X,r)*P)*h2(X(i,:),X(j,:),r);
        else
            Q(i,j) =  2*g*(1-P(i))*(c0 + hvector(i,X,r)*P)*h2(X(i,:),X(j,:),r);
        end
    end
end
```

Where hvector is defined as:

```
function v = hvector(i,X,r)
    v = zeros(1,900);
```

```
    for j = 1:900
        if i == j
            v(j) = 0;
        else
            v(j) = h2(X(i,:),X(j,:),r);
        end
    end
end
function f = h2(xi,xj,r)
    l = 3;
    f = r*exp(-norm(xi-xj)^2/l^2);
end
```

To compute the matrix eigenvectors and eigenvalues, we use the already implemented function in the matlab packages:

```
[VEPS,VAPS] = eig(Q);
```

References

[1] Mitchell, J. R., & Wang, J. J. (2014). Expanding application of the Wiggers diagram to teach cardiovascular physiology. Advances in physiology education, 38(2), 170-175.

[2] Matsuoka, S., & Hilgemann, D. W. (1992). Steady-state and dynamic properties of cardiac sodium-calcium exchange. Ion and voltage dependencies of the transport cycle. The Journal of General Physiology, 100(6), 963-1001.

[3] Gao, W. D., Atar, D., Backx, P. H., & Marban, E. (1995). Relationship between intracellular calcium and contráctile force in stunned myocardium direct evidence for decreased myofilament Ca2+ responsiveness and altered diastolic function in intact ventricular muscle. Circulation Research, 76(6), 1036-1048.

[4] Mackay, J., Mensah, G. A., Mendis, S., & Greenlund, K. (2004). The atlas of heart disease and stroke. World Health Organization.

[5] Beuckelmann, D. J., Näbauer, M., & Erdmann, E. (1992). Intracellular calcium handling in isolated ventricular myocytes from patients with terminal heart failure. Circulation, 85(3), 1046-1055.

[6] Cheng, H., & Lederer, W. J. (2008). Calcium sparks. Physiological reviews, 88(4), 1491-1545.

[7] Hernandez-Hernandez, G., Alvarez-Lacalle, E., & Shiferaw, Y. (2015). Role of connectivity and fluctuations in the nucleation of calcium waves in cardiac cells. Physical Review E, 92(5), 052715.

[8] MacGowan, G. A., Kirk, J. A., Evans, C., & Shroff, S. G. (2006). Pressure-calcium relationships in perfused mouse hearts. American Journal of Physiology-Heart and Circulatory Physiology, 290(6), H2614-H2624.

[9] Baddeley, D., Jayasinghe, I. D., Lam, L., Rossberger, S., Cannell, M. B., & Soeller, C. (2009). Optical single-channel resolution imaging of the ryanodine receptor distribution in rat cardiac myocytes. Proceedings of the National Academy of Sciences, 106(52), 22275-22280.